Electric versus Gasoline Vehicle Particulate Matter and Greenhouse Gas Emissions: Large-scale Analysis

Hesham A. Rakha (Corresponding author)

Charles E. Via, Jr. Department of Civil and Environmental Engineering
Center for Sustainable Mobility, Virginia Tech Transportation Institute
3500 Transportation Research Plaza, Blacksburg, VA 24061
Phone: (540) 231-1505; Fax: (540) 231-1555
hrakha@vt.edu
ORCID number: 0000-0002-5845-2929

Mohamed Farag

Center for Sustainable Mobility, Virginia Tech Transportation Institute
3500 Transportation Research Plaza, Blacksburg, VA 24061
Phone: (540) 231-1500 Fax: (540) 231-1555
mmagdy@vt.edu
ORCID number: 0000-0002-3084-0815

Hosein Foroutan

Charles E. Via, Jr. Department of Civil and Environmental Engineering
Phone: (540) 232-8400
hosein@vt.edu
ORCID number: 0000-0003-4185-3571

ABSTRACT

This study addresses the contentious issue of non-exhaust particulate matter (PM) emissions from battery electric vehicles (BEVs) compared to internal combustion engine vehicles (ICEVs) by developing models to quantify tire and brake PM emissions and incorporate them in a microscopic traffic simulation environment. Furthermore, exhaust greenhouse gas (GHG) emissions are quantified to develop a comprehensive picture of vehicle network emissions. The key findings are: 1) BEVs emit more tire and less brake PM emissions, thus necessitating a comprehensive analysis to avoid erroneous conclusions. 2) If at least 15% of travel is city driving, BEVs produce less non-exhaust PM emissions. 3) For the freeway section analyzed, a volume-to-capacity ratio of at least 0.25 is required for BEVs to produce less non-exhaust PM emissions. By incorporating these detailed models into traffic simulations, the study provides a tool for policymakers to better understand and manage vehicle emissions at a city level.

Keywords: Non-exhaust emissions; particulate matter emissions; tire emissions; brake emissions; battery electric vehicles; large-scale traffic modeling.

1. INTRODUCTION

This section describes the extant literature on particulate matter (PM) emissions and this study's contributions to advancing the state of the art in network-wide modeling of non-exhaust PM emissions via the development of a novel tool. Developing such a tool is necessary to assess the network-wide environmental impact of various intelligent transportation system (ITS) applications.

1.1 Literature Review

Airborne particulate matter (PM) is recognized as one of the main risk factors for adverse health effects and premature deaths worldwide, and road traffic has long been viewed as a major contributor to PM pollution (Kim, Kabir and Kabir 2015, Alemayehu, Asfaw and Terfie 2020, Sisani, Di Maria and Cesari 2022). Traffic-related PM is classified into exhaust emissions, which are the result of fuel combustion, and non-exhaust emissions, which are caused by tire and brake abrasion. Vehicle exhaust emissions have been decreasing considerably due to advances in technology, vehicle electrification, and stricter regulations. In contrast, so far unregulated non-exhaust emissions have been increasing with rising road transport activities. Therefore, quantifying non-exhaust emissions, pertaining to both internal combustion engine vehicles (ICEVs) and battery electric vehicles (BEVs), has been the subject of many recent studies (see review articles (Timmers and Achten 2016, Harrison, et al. 2021, Piscitello, et al. 2021).

The complexity in quantifying the difference between non-exhaust emissions of ICEVs and BEVs arises from the fact that BEVs are expected to generate more tire wear particles (TWPs) due to an increase in vehicle mass, while they emit fewer brake wear particles (BWPs) thanks to the regenerative braking system—a mechanism that uses the spinning wheel's kinetic energy during braking to recharge the battery. Moreover, the emission of both TWPs and BWPs is sensitive to environmental and driving conditions in highway, city, or rural areas. The dependency of TWPs and BWPs on vehicle mass has been studied by Oroumiyeh & Zhu (2021) and (Beddows and Harrison 2021). The latter study further investigated the implications of their findings for BEVs and concluded that up to a 24% reduction in overall PM emissions for BEVs is possible if proper regenerative braking is used. The importance of a regenerative braking system in reducing PM emissions in BEVs was also recently emphasized by (Bondorf, et al. 2023) and (Zhang, et al. 2024).

The majority of studies in this area have mainly focused on sampling non-exhaust PM either in a laboratory setup (Zhang, et al. 2024) or in road tests (Oroumiyeh and Zhu 2021) and analyzing samples using a variety of instruments to understand their emission rate, particle size distribution, and elemental/organic composition (Alves, et al. 2020, Rødland, et al. 2023). Total PM emission rates (often in units of mg/km) have then been estimated for a single tire or vehicle (Zhang, et al. 2024, Rødland, et al. 2023). Nevertheless, there is a gap in the literature in incorporating this knowledge into estimating vehicle PM emissions varying with mass, acceleration / deceleration levels, and traffic conditions.

1.2 Paper Contribution

This research makes three key contributions to the state of the art in vehicle emission modeling. First, it introduces new emission models that are sensitive to the vehicle's mass and deceleration level for more accurate quantification of TWP and BWP emissions, which are

critical factors in comparing the environmental impact of BEVs and ICEVs. Second, the developed brake and tire emission models have been incorporated into microscopic traffic simulation software to result in a novel tool; this tool is capable of conducting network-wide assessments of both vehicle exhaust and non-exhaust emissions, thereby offering a comprehensive view of the emissions landscape. Third, using the developed tool, this study has produced the first network-wide assessment and comparison of exhaust and non-exhaust emissions associated with BEVs and ICEVs. This enables a detailed analysis of how these vehicles perform under various traffic conditions and demand levels, providing valuable insights for policymakers and transportation planners.

2. MODEL DEVELOPMENT

This section describes the models developed to quantify vehicle energy consumption and brake and tire PM emissions. Considering their health implications, we focused on $PM_{2.5}$ (PM with a diameter of less than 2.5 microns). Moreover, we have presented the modeling approach to calculate greenhouse gas (CO_2) emissions from a vehicle's exhaust. The computation of the vehicle's power is described first, given its criticality to modeling vehicle fuel/energy consumption, tailpipe emissions, and brake PM emissions in BEVs.

2.1 Vehicle Fuel/Energy Consumption Modeling

The modeling of ICEV fuel consumption in the INTEGRATION software (Rakha, 2024a, Rakha, 2024b, Rakha et al., 2012, Rakha and Zhang, 2004, Rakha and Ahn, 2004) (Farag, et al. 2021) is conducted using the Virginia Tech Comprehensive Power-based Fuel Consumption Model (VT-CPFM) (Rakha et al., 2011). The modeling of electric vehicle energy consumption is achieved using the VT-CPEM model that is an extension of the model described in (Fiori et al., 2016) with some modifications and is also currently implemented in the INTEGRATION software.

The computation of energy consumption is executed each second by computing the vehicle's power consumption at the wheels using Eqn. (1). The power at the tank is then computed by accounting for all losses within the vehicle while moving from the wheels to the tank/battery depending on the powertrain type as shown in Eqn. (2).

$$P_w(t) = \big(R(t) + ma(t)\big) \times v(t) \tag{1}$$

$$P_t(t) = P_a + \frac{P_w(t)}{\eta_o} \tag{2}$$

Here $P_w(t)$ is the power applied at the vehicle wheels over period $t - \Delta t$ through t; $R(t)$ is the total resistance force acting on the vehicle during the same time interval, which includes the aerodynamic, rolling and grade resistance forces; m is the vehicle mass; $a(t)$ is the vehicle acceleration over the analysis time step, Δt; $v(t)$ is the average vehicle speed over the analysis time step, Δt; $P_t(t)$ is the power exerted at the tank/battery over the time step, Δt; P_a is the auxiliary power exerted o.ver the time step, Δt; η_o is the overall efficiency. In the case of electric vehicles, this includes the efficiency of the driveline, the electric motor, and the battery. In the case of an ICEV, this typically equals 0.92, and for a BEV, it is 0.78 (0.95×0.91×0.90), as was described in (Fiori, Ahn and Rakha 2016).

Once the power at the tank/battery is computed, the fuel/energy consumption in ml or kWh is computed using a second-degree polynomial function of power in units of kW, as shown in Eqns. (3) and (4). In the case of BEVs negative powers are used to regenerate the vehicle's battery, as shown in Eqn. (4).

$$FC(t) = \begin{matrix} (\alpha_0 + \alpha_1 P_t(t) + \alpha_2 P_t^2(t))\Delta t & \forall\, P_w(t) \geq 0 \\ \alpha_0 \Delta t & \forall\, P_w(t) < 0 \end{matrix} \tag{3}$$

$$EC(t) = \begin{matrix} \left(\alpha_0 + \alpha_1 \frac{P_w(t)}{\eta_o} + \alpha_2 \left(\frac{P_w(t)}{\eta_o}\right)^2\right)\Delta t & \forall\, P_w(t) \geq 0 \\ \left(\alpha_0 - \left(\alpha_1 |P_w(t)| + \alpha_2 \left(P_w(t)\right)^2\right)\eta_{rb}\eta_o\right)\Delta t & \forall\, P_w(t) < 0 \end{matrix} \tag{4}$$

Here the α_0, α_1, and α_2 parameters are calibrated using the Environmental Protection Agency (EPA) city and highway ratings, as was presented in (H. A. Rakha, K. Ahn, et al. 2011) and Δt is the time step duration in seconds. The variable η_{rb} is the regenerative braking efficiency, which is taken to be 1.0 in this case. In the case of ICEVs the α_0 parameter is computed as shown in Eqn. (5).

$$\alpha_0 = \frac{p_m \omega_i D}{22164 Q N} \tag{5}$$

Here the variable p_m represents the idling fuel mean pressure (400,000 Pa); ω_i is the engine's idling speed (rpm); D is the engine displacement (liters); Q is the fuel lower heating value (43,000,000 J/kg for gasoline fuel); and N is the number of engine cylinders.

Alternatively, in the case of a BEV, the α_0 parameter in units of kWh/s is computed using Eqn. (6).

$$\alpha_0 = \frac{P_a}{3600} \tag{6}$$

2.2 Brake PM Emission Modeling

The EPA MOtor Vehicle Emission Simulator (MOVES) is an emission modeling system that estimates mobile source emissions at different levels, including national, county, and project for various air pollutants (EPA 2014). The latest version of the model is the MOVES4 model, which provides a model for the computation of brake $PM_{2.5}$ emissions ($PM_{2.5}^b(t)$) at time step t in g/h as demonstrated in Eqn. (7) considering a discrete approximation of the continuous motion of a vehicle.

$$PM_{2.5}^b(t) = 0.1872 d(t)^{3.195} \tag{7}$$

Here $d(t)$ is the deceleration level of the vehicle over the period t and $t - \Delta t$ in m/s^2 ($d(t) = |a(t)|\ \forall\ a(t) < 0$). Consequently, the brake $PM_{2.5}$ emissions in mg/s can then be computed as demonstrated in Eqn. (8).

$$PM_{2.5}^{b}(t) = 0.052d(t)^{3.195} \quad (8)$$

Using data provided in the MOVES4 model (Table I) we fit a linear regression line between $PM_{2.5}$ emissions and vehicle mass. The model coefficients were then normalized by dividing by the corresponding $PM_{2.5}$ emissions considering the average mass of a light duty vehicle (1479 kg) to compute a mass emission correction factor (CF_m).

Table I. Data from the MOVES model

Mass [kg]	$PM_{2.5}$ [g/h]	$PM_{2.5}$ [mg/s]	CF_m
285	0.355	0.099	0.64
1,479	0.558	0.155	1.00
1,904	0.631	0.175	1.13
1,952	0.639	0.178	1.14
8,550	1.760	0.489	3.16
12,940	2.510	0.697	4.50
22,809	4.190	1.164	7.51
16,556	3.120	0.867	5.60
22,809	4.190	1.164	7.51

The vehicle mass correction factor was derived as shown in Eqn. (9).

$$CF_m = 0.548782 + 0.000305m \quad (9)$$

Here m is the vehicle mass in kilograms. This equation ensures that the correction factor equals 1.0 for a light duty vehicle mass of 1479 kg.

The final model for computing brake $PM_{2.5}$ emissions can then be written as described in Eqn. (10).

$$PM_{2.5}^{b}(t) = 0.052 \times (0.548782 + 0.000305m) \times d(t)^{3.195} \quad (10)$$

In the case of BEVs, regenerative braking is applied when the power is negative and greater than a certain threshold. Consequently, BEV $PM_{2.5}$ emissions are zero when the vehicle is decelerating and the power at the wheels is greater than or equal to the minimum power (P_{min}). P_{min} is computed using a C factor that is typically set between 0.8 and 1.2 hours where P_{min} is computed using Eqn. (11).

$$P_{min} = -\frac{BS}{C} \quad (11)$$

Here BS is the battery size in kWh and C is the duration of time for the battery to deplete given the current power demand, typically taken to be in the range of 0.8 to 1.2 hours. In this study, we used the average C value of 1.0 hour.

In our analysis, we assumes that the vehicle first uses its regenerative braking and that any extra braking beyond the regenerative charging limits is assigned to the mechanical braking system. Consequently, when the power at the wheels ($P_w(t)$) at instant t is less than P_{min}, the braking acceleration that is assigned to the brake pads is computed as shown in Eqn. (12).

$$d_p(t) = \frac{P_w(t) - P_{min}}{P_w(t)} \times d(t) \tag{12}$$

The $PM_{2.5}$ emissions emitted by the BEV brakes is finally computed using Eqn. (13).

$$PM_{2.5}^b(t) = \begin{cases} 0 & d(t) > 0 \quad P_w(t) \geq P_{min} \\ 0.052 C F_m \left(\frac{P_w(t) - P_{min}}{P_w(t)} d(t) \right)^{3.195} & d(t) > 0 \quad P_w(t) < P_{min} \end{cases} \tag{13}$$

This equation ensures that the battery can receive the regenerative power and that the remainder of the power is provided by the brake pads. The implicit assumption in this model is that the deceleration associated with the brake pads is directly proportional to the power remaining after accounting for regenerative braking.

2.3 Tire PM Emission Modeling

The MOVES4 model provides an equation for computing the tire weight loss (TWL) in g/mi as shown in Eqn. (14).

$$TWL = 0.2158 e^{-\frac{0.015v}{1.6}} \tag{14}$$

Here $v(t)$ is the average vehicle speed over the time interval $t - \Delta t$ to t in km/h.

Studies have shown that PM_{10} emissions constitute approximately 8% of the TWL emissions and that PM_{10} emissions are 6.82 times $PM_{2.5}$ emissions based on the data collected by (Zhang, et al. 2024). Consequently, the $PM_{2.5}$ emissions in mg/s can be computed by multiplying the previous equation by the vehicle speed and applying the corresponding conversion factors results in Eqn. (15).

$$PM_{2.5}^t(t) = 0.2158 e^{-\frac{0.015v(t)}{1.6}} \times \frac{0.08 \times v(t)}{1.6 \times 3.6 \times 6.82} \tag{15}$$

This reduces to Eqn. (16).

$$PM_{2.5}^t(t) = 0.000439579 \times v(t) \times e^{-0.009375v(t)} \tag{16}$$

This reveals an exponential relationship between tire $PM_{2.5}$ emissions and vehicle speed.

A recent paper by Zhang et al. (Zhang, et al. 2024) collected data on tire emissions for a total of nine tires that support different maximum loads, as shown in Table II.

Table II. Data collected as part of the Zhang et al. (2024) study (Zhang, et al. 2024)

Tire	Max Load [kg]	Mass [kg]	$PM_{2.5}$ [mg/km]			$PM_{2.5}$ [mg/h]
			F	R	Total	
1	500	1600	0.095	0.095	0.190	9.5
2	650	2080	0.090	0.090	0.180	9.0
3	850	2720	0.055	0.055	0.110	5.5
4	1060	3392	0.058	0.055	0.113	5.6
5	615	1968	0.070	0.060	0.130	6.5
6	850	2720	0.060	0.050	0.110	5.5
7	1060	3392	0.070	0.075	0.145	7.3
8	750	2400	0.040	0.040	0.080	4.0
9	800	2560	0.055	0.050	0.105	5.3

Tires 1 through 4 are snow tires, while Tires 5 through 9 are all-season tires. Among the all-season tires, only the behavior of tire 5 seemed suspicious (generated far more $PM_{2.5}$ than the other all-season tires[1]) so it was removed from the analysis. We then computed the $PM_{2.5}$ and PM_{10} emissions on a per second basis. These values were then used to calculate the correction factor for the vehicle mass. Using these data we found the average ratio of $PM_{10}/PM_{2.5}$ to be 6.82.

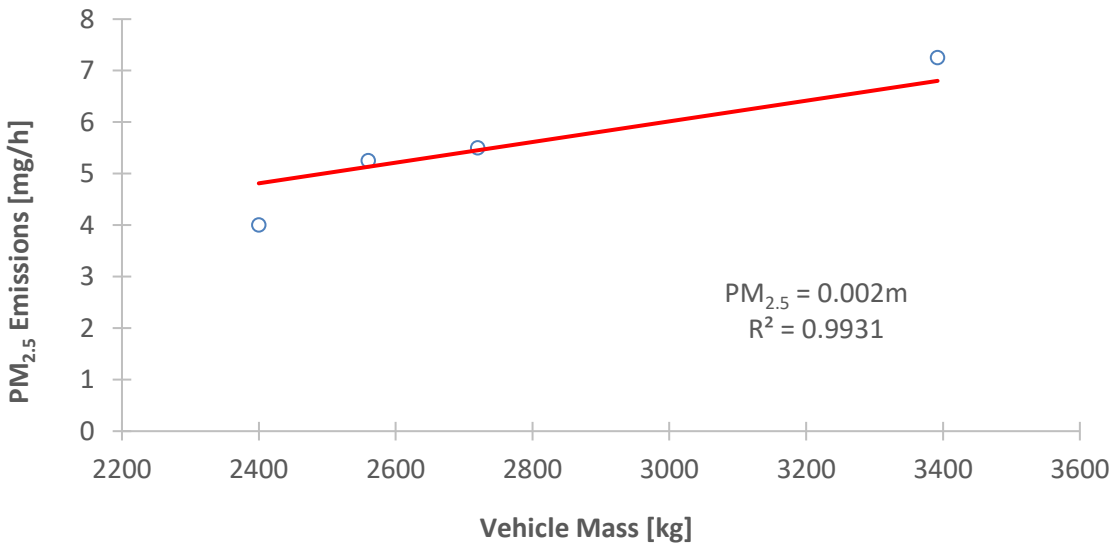

Figure 1. $PM_{2.5}$ emissions as a function of vehicle mass for all-season tires (Zhang et al., 2024)

Fitting a linear model to the data, we obtain the relationship between $PM_{2.5}$ emissions and the vehicle mass, as shown in Figure 1. Initially, we tried the model with an intercept, but the

[1] We reached out to the authors to understand why tire 5 is an outlier but received no response. Therefore, due to the lack of information about the tire type, we decided to remove tire 5 from our analysis and focus on tires 6-9 to develop a simple model relating tire emissions to the exerted load.

intercept was found to be statistically insignificant, therefore we used a model without an intercept, as shown in Eqn. (17). The regression results are presented in the Appendix.

$$PM_{2.5}^{t} = 5.5695 \times 10^{-7} m \tag{17}$$

A correction factor for the vehicle mass was then derived as shown in Eqn. (18). This correction factor produces results consistent with field measurements conducted by Emissions Analytics (2024), which indicated that tire wear emissions were 26% greater from the Tesla model Y BEV compared to the Kia Niro hybrid electric vehicle (HEV) that was 32% lighter, as discussed in the following section (Emissions_Analytics 2024). This finding shows that the proposed mass adjustment factor produces corrections consistent with empirical field measurements (see Figure 2).

$$CF_m = \frac{m}{1479} \tag{18}$$

The final model is then formulated as shown in Eqn. (19).

$$PM_{2.5}^{t}(t) = 2.97213 \times 10^{-7} \times v(t) \times m \times e^{-0.009375 v(t)} \tag{19}$$

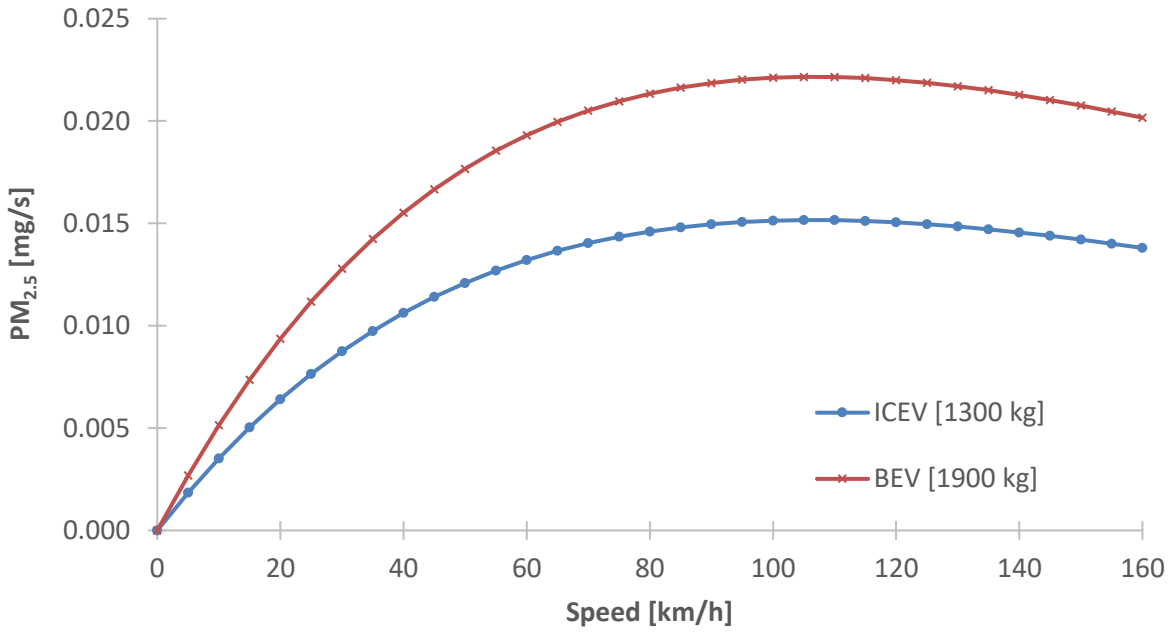

Figure 2. Variation in $PM_{2.5}$ tire emissions for an average ICEV and BEV

The total $PM_{2.5}$ emissions are then computed as shown in Eqn. (20).

$$PM_{2.5}(t) = PM_{2.5}^{b}(t) + PM_{2.5}^{t}(t) \tag{20}$$

PM_{10} can then be computed by scaling the $PM_{2.5}$ emissions by a factor of 6.82 based on field measurements conducted by Zhang et al. as shown in Eqn. (21).

$$PM_{10}(t) = PM_{2.5}(t) \times 6.82 \quad (21)$$

2.4 Exhaust PM and CO_2 Emission Modeling

As mentioned, in an earlier study conducted by Emissions Analytics (Emissions_Analytics 2024), tire and tailpipe emissions from a Kia Niro HEV and a Tesla Model Y BEV were measured in the field. During testing the vehicles traveled in a group to eliminate external factors including driving style and weather conditions. The Kia was instrumented with a tailpipe portable emissions measurement system (PEMS) to measure tailpipe emissions, and the Tesla was instrumented with an equivalent mass to ensure equal masses in the vehicles. The test cycle was made up of five repetitions of a standard Emissions Analytics drive cycle, totaling 741 km. Throughout the test, the wheels were dismounted, cleaned, weighed and remounted to calculate the mass loss. The study reported that the Kia Niro HEV showed almost no tailpipe pollutants except for CO_2 emissions. Specifically, the study noted that there were almost no tailpipe emissions from the Kia except for CO_2. This is caused by the use of a particulate filter that reduces PM to almost zero. Based on these findings, the following assumptions are made for the current study: 1) Exhaust $PM_{2.5}$ emissions from gasoline ICEVs are assumed to be negligible and effectively zero, given the efficiency of modern particulate filters. 2) The study primarily models CO_2 emissions from gasoline ICEVs due to their significant impact on climate change.

The CO_2 emissions are directly proportional to fuel consumption rates, as was demonstrated in an earlier paper (H. A. Rakha, K. Ahn, et al. 2011). Specifically, CO_2 emissions can be estimated using the carbon balance equation from the burning of fuel and considering the carbons in hydrocarbon (HC) and carbon monoxide (CO) emissions. Given that the value of CO_2 emissions is substantially larger than HC and CO emissions, CO_2 emissions are primarily directly proportional to the fuel consumption level. The study demonstrated that for every liter of regular gasoline fuel burned, 2330 grams of CO_2 emissions are emitted. Consequently, CO_2 emissions are computed using a constant conversion factor of 2330 grams for every liter of fuel consumed.

3. CITY-LEVEL PARTICULATE MATTER QUANTIFICATION

The brake and tire PM emission models that were developed and described above were then incorporated in the INTEGRATION microscopic traffic simulation software to compute non-exhaust PM emissions. Tailpipe PM emissions from ICEVs and BEVs were assumed to be zero, based on empirical observations, as discussed.

This section first describes the INTEGRATION software and then describes how these models were incorporated in the software and how network-wide emissions are computed.

It should be noted that because the INTEGRATION software uses a point mass vehicle dynamics model, it not only captures the effect of vehicle mass on non-exhaust PM emissions, but also captures differences in vehicle trajectories caused by variances in vehicle characteristics and thus presents a novel and realistic assessment of vehicle non-exhaust and exhaust emissions. A more detailed description of the longitudinal vehicle motion modeling approach is provided in the next section given that it is essential to the modeling of vehicle emissions.

3.1 INTEGRATION Traffic Modeling Framework

INTEGRATION is microscopic traffic assignment and simulation software developed and maintained at the Center for Sustainable Mobility (CSM) (Farag, et al. 2021). INTEGRATION was first established in the late 1980s, with developments and enhancements continuing through today. It was conceived as an integrated simulation and traffic assignment model and performs traffic simulations by tracking the movement of individual vehicles every 1/10th of a second. This allows the detailed analysis of lane-changing and longitudinal vehicle movements and their resulting shock wave propagations. It also permits considerable flexibility in representing spatial and temporal variations in traffic conditions. The INTEGRATION software incorporates a point mass vehicle dynamics model that computes the vehicle's tractive effort, aerodynamic, rolling, and grade-resistance forces. The vehicle dynamics model is fully integrated in the car-following model (Fadhloun et al., 2017, Wang et al., 2017a, Fadhloun and Rakha, 2019, Wang et al., 2017b). In addition to estimating stops and delay (Dion, Rakha and Kang 2004, Rakha, Kang and Dion, Estimating vehicle stops at undersaturated and over saturated fixed-time signalized intersections 2001) the model can also estimate the crash risk (Avgoustis, Rakha and Van Aerde 2004), the fuel consumed by vehicles (Rakha and Ahn, Integration modeling framework for estimating mobile source emissions 2004, H. A. Rakha, K. Ahn, et al. 2011) and the vehicular emissions. The INTEGRATION model has not only been validated against standard traffic flow theory (Rakha et al., 2001, Dion et al., 2004), but has also been used to evaluate large-scale real-life applications (Elbery, et al. 2018, Du, et al. 2018).

A key component of the INTEGRATION software related to this effort is the modeling of the vehicle's longitudinal motion. This modeling is achieved using the Fadhloun-Rakha car-following model (Fadhloun and Rakha, A novel vehicle dynamics and human behavior car-following model: Model development and preliminary testing 2019). The Fadhloun-Rakha model includes two terms, one for acceleration and one for collision avoidance when approaching slower vehicles, as shown in Eqn. (22). Here the index n refers to the subject vehicle and the index $n-1$ refers to the vehicle directly ahead of the subject vehicle in the same lane. Furthermore, d_{des} is the desired deceleration; g is the gravitational deceleration, which is equal to 9.81 m/s^2; G is the roadway grade; $s_n(t)$ is the spacing between vehicle n and vehicle $n-1$ at instant t; and s_j is the jam density spacing between vehicles. It should be noted that the spacing is the sum of the length of the vehicle plus the distance from the front bumper of the following vehicle and the rear bumper of the lead vehicle. It should be noted that the collision avoidance component ensures that the vehicle maintains a safe distance that would allow it to decelerate at the desired deceleration to avoid a collision with the vehicle ahead of it.

$$a_n(t) = \begin{cases} f_p(t) \times a_n^{max}(t) & \forall\, X_n(t) \le 1 \\ \dfrac{\left[v_n(t)^2 - v_{n-1}(t)^2 - \sqrt{(v_n(t)^2 - v_{n-1}(t)^2)^2}\right]^2}{16 \times d_{des} \times \left(s_n(t) - s_j\right)^2} & \forall\, X_n(t) > 1 \end{cases} \quad (22)$$

In the case of acceleration Eqn. (2222) incorporates the driver's throttle input ($f_p(t)$) at instant t multiplied by the maximum vehicle acceleration (a_{max}) computed using a point mass vehicle dynamics model as shown in Eqn. (23). Here $F_n(t)$ is the subject vehicle's tractive force, which is a function of the vehicle power and the maximum sustainable force between the vehicle wheels and the roadway surface. $R_n(t)$, which was defined earlier, is the total resistance force

acting on the vehicle. The interested reader can refer to (Fadhloun and Rakha, A novel vehicle dynamics and human behavior car-following model: Model development and preliminary testing 2019) for more information on how $F_n(t)$ and $R_n(t)$ are computed.

$$a_{max} = \frac{(F_n(t) - R_n(t))}{m} \tag{23}$$

The driver throttle input at instant t ($f_p(t)$) is computed using Eqn. (24) in conjunction with Eqn. (25).

$$f_p(t) = e^{-g_1 X_n(t)}\left(1 - X_n(t)^{g2} e^{g_2(1-X_n(t))}\right)^{g_3} \tag{24}$$

$$X_n(t) = \frac{\min\left(\tilde{s}_n(t), \tilde{s}_n(0.99v_f)\right)}{\min\left(s_n(t), \tilde{s}_n(0.99v_f)\right)} \cdot \frac{v_n(t)}{\tilde{v}_n(t)} \tag{25}$$

Eqn. (25) ensures that the driver/vehicle converges to the steady-state fundamental diagram spacing ($\tilde{s}_n(t)$) and velocity ($\tilde{v}_n(t)$). The parameters g_1, g_2, and g_3 are driver-specific parameters that characterize the aggressiveness of the driver on the accelerator pedal. The model uses the Van Aerde steady-state spacing derived from the fundamental diagram (H. A. Rakha, Validation of Van Aerde's Simplified Steady-state Car-following and Traffic Stream Model 2009) that is presented in Eqn. (2628). The steady-state speed ($\tilde{v}_n(t)$) is computed by replacing the steady-state spacing $\tilde{s}_n(t)$ with the actual spacing $s_n(t)$ and solving for the steady-state speed ($\tilde{v}_n(t)$) as shown in Eqn. (29).

$$\tilde{s}_n(t) = c_1 + \frac{c_2}{(v_f - v_n(t))} + c_3 v_n(t) \tag{26}$$

The steady-state car-following parameters c_1, c_2, and c_3 are computed from the fundamental diagram parameters: namely, the roadway free-flow speed, u_f (km/h); the speed-at-capacity, u_c (km/h); the roadway saturation flow rate, q_c (veh/h); and the roadway jam density, k_j (veh/km), which is the inverse of the jam density spacing s_j, as shown in Eqn. (27) (H. A. Rakha, Validation of Van Aerde's Simplified Steady-state Car-following and Traffic Stream Model 2009). The Van Aerde fundamental diagram thus needs four parameters to be calibrated for a specific roadway segment: u_f, u_c, q_c, and k_j (Rakha and Arafeh, Calibrating Steady-State Traffic Stream and Car-following Models using Loop Detector Data 2009).

$$c_1 = \frac{u_f}{k_j u_c^2}\left(2u_c - u_f\right) \quad c_2 = \frac{u_f}{k_j u_c^2}\left(u_f - u_c\right)^2 \quad c_3 = \frac{1}{q_c} - \frac{u_f}{k_j u_c^2} \tag{27}$$

For conditions where the lead vehicle is traveling at a higher velocity (non-steady-state conditions), then the desired safe following spacing can be calculated using Eqn. (28). This formulation permits the driver to drive at a spacing smaller than the steady-state spacing when the vehicle ahead of it is driving at a greater speed.

$$\tilde{s}_n(t) = \max\left(c_1 + \frac{c_2}{(v_f - v_n(t))} + c_3 v_n(t) - \frac{v_{n-1}(t)^2 - v_n(t)^2 - \sqrt{(v_{n-1}(t)^2 - v_n(t)^2)^2}}{4d_{des}}, \frac{L_n + 1}{1000}\right) \quad (28)$$

Here L_n is the length of vehicle n in meters. The steady-state vehicle speed ($\tilde{v}_n(t)$) is computed using Eqn. (29).

$$\tilde{v}_n(t) = \frac{-c_1 + c_3 v_f + s_n(t) - \sqrt{\left(c_1 - c_3 v_f - s_n(t)\right)^2 - 4c_3\left((s_n(t) - c_1)v_f - c_2\right)}}{2c_3} \quad (29)$$

The vehicle car-following model is applied every decisecond to compute the vehicle acceleration and speed, which are then fed into the emission models described earlier every second to compute vehicle emissions.

3.2 City-level Non-exhaust $PM_{2.5}$ Quantification

As part of this effort the INTEGRATION software was extended to incorporate the brake and tire $PM_{2.5}$ and PM_{10} emissions. In doing so the model computes the brake and tire $PM_{2.5}$ emissions every second based on the average speed and acceleration over the previous 1-second time step, as shown in Eqn. (30). The total $PM_{2.5}$ emissions are then computed by summing the $PM_{2.5}$ emissions over the entire trip duration ($T_i = T_e - T_0$) for vehicle n. The network-wide $PM_{2.5}$ emissions are then computed by summing across all the vehicles (V) within the simulation run. This bottom-up approach ensures that emissions are computed accurately by capturing all the transient behavior of the vehicle as it travels in the computation of network-wide emissions.

$$PM_{2.5} = \sum_{n=1}^{V} \sum_{t=T_0}^{T_e} PM_{2.5}^{n}(t) \quad (30)$$

4. RESULTS AND ANALYSIS

For this section, we used the brake and tire $PM_{2.5}$ and PM_{10} models to investigate the difference in PM emissions for BEVs compared to ICEVs. This analysis was first conducted on a single vehicle for three drive cycles and then quantified using the INTEGRATION model on a sample freeway network selected to favor ICEVs, given that no control devices were in place to force the vehicles to stop and given that the terrain is mountainous.

4.1 Typical Weights of ICEVs and BEVs

Prior to conducting the single vehicle powertrain comparison, it was important to quantify the typical weights of BEVs and ICEVs for use in the analysis. Table III presents the summary characteristics of different BEVs, ICEVs, and HEVs sold in the United States. As indicated, the typical BEV is approximately 43% heavier than its counterpart ICEV. Alternatively, HEVs are approximately 29% heavier than their counterpart ICEVs. Using these results, simulations were conducted assuming a weight of 1300 kg for ICEVs and 1900 kg for BEVs.

Table III. Powertrain vehicle comparison

Vehicle	Type	Vol. [ft³]	Wgt. [lb]	Avg. Wgt. [kg]	Diff. [%]

Tesla Model 3	BEV	435	3650	1905	43%
Hyundai Ioniq 5	BEV	491	4050		
Polestar 2	BEV	431	4600		
BMW i4	BEV	453	4450		
Audi Q4 e-tron	BEV	487	4250		
Volvo XC40 Recharge	BEV	491	4700		
Volkswagen ID.4	BEV	480	4350		
Chevrolet Bolt EV	BEV	413	3550		
Hyundai Elantra	ICEV	416	2850	1328	0%
Kia Forte	ICEV	426	2850		
Honda Civic	ICEV	419	2900		
Toyota Corolla	ICEV	415	2950		
Nissan Sentra	ICEV	440	2950		
Mazda3	ICEV	421	3000		
Volkswagen Jetta	ICEV	433	3150		
Subaru Impreza	ICEV	434	3150		
Ford Focus	ICEV	424	2950		
Nissan Versa	ICEV	410	2600		
Chevrolet Sonic	ICEV	402	2850		
Ford Edge	HEV	574	4200	1712	29%
BMW 3 Series	HEV	426	3650		
Audi A4	HEV	434	3600		
Mercedes-Benz C-class	HEV	426	3650		
Volvo S60	HEV	436	3750		

4.2 Single Vehicle Comparative Analysis

We ran the model on three cycles: the EPA city cycle, the EPA highway cycle, and the US06 cycle. The speed profiles of the three cycles are provided in Figure 3, Figure 4, and Figure 5, respectively. The results of the analysis are summarized in Table IV. The different driving cycles showed mixed results. In the case of the EPA city and US06 cycles, where braking is more frequent, the BEVs are more efficient with a reduction in $PM_{2.5}$ non-exhaust emissions of 45% and 61%, respectively. Alternatively, in the case of the highway drive cycle, the BEV emits 25% more $PM_{2.5}$ non-exhaust emissions, which is caused by the heavier vehicle mass of BEVs relative to ICEVs.

Table IV. $PM_{2.5}$ emissions for ICEVs and BEVs on three different driving cycles [mg]

	ICEV [mg]			BEV [mg]			Change [%]
	Brake	Tire	Total	Brake	Tire	Total	
City	25.2	15.2	40.4	0.0	22.3	22.3	-45%
Hwy	1.8	10.8	12.6	0.0	15.8	15.8	25%
US06	26.5	7.4	33.9	2.5	10.8	13.3	-61%

To identify the reasons behind these different outcomes, Table V summarizes the characteristics of each of the drive cycles. It appears that what distinguishes the highway cycle is the combination of the higher average speed and lower percentage of deceleration and negative power events (only 11% of the total observations).

Table V: Characteristics of the three driving cycles

	Avg. Speed [km/h]	Min. Accel [m/s²]	Max. Accel [m/s²]	Decelerating [%]
City	34	-1.47	1.47	24%
Hwy	77	-1.47	1.42	11%
US06	77	-2.76	2.88	23%

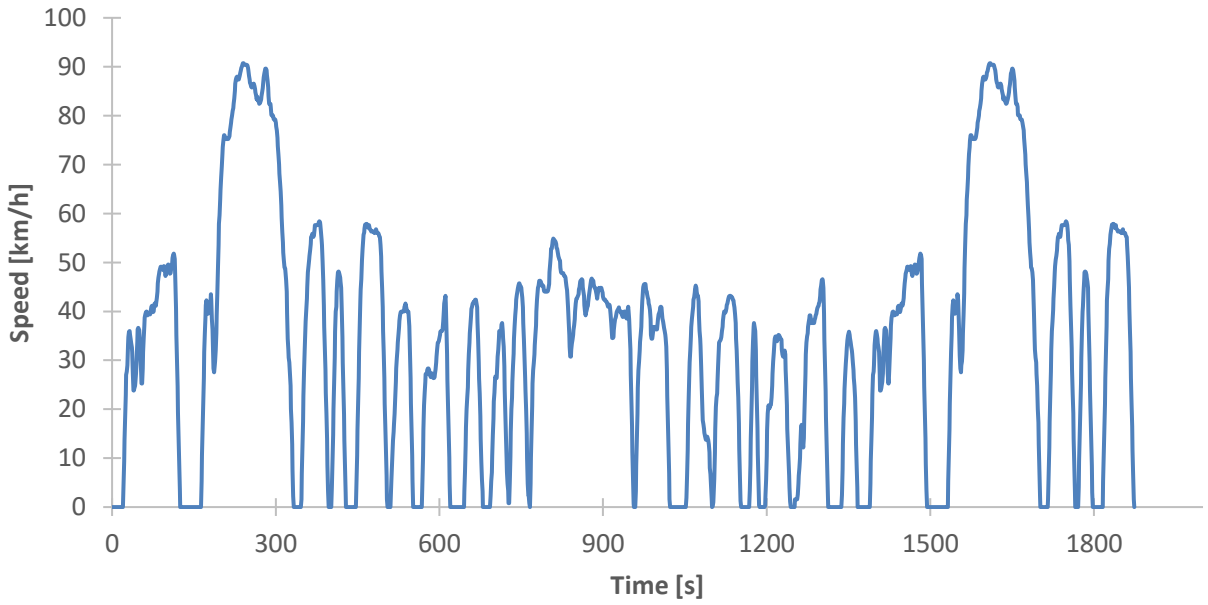

Figure 3: Speed profile of City drive cycle

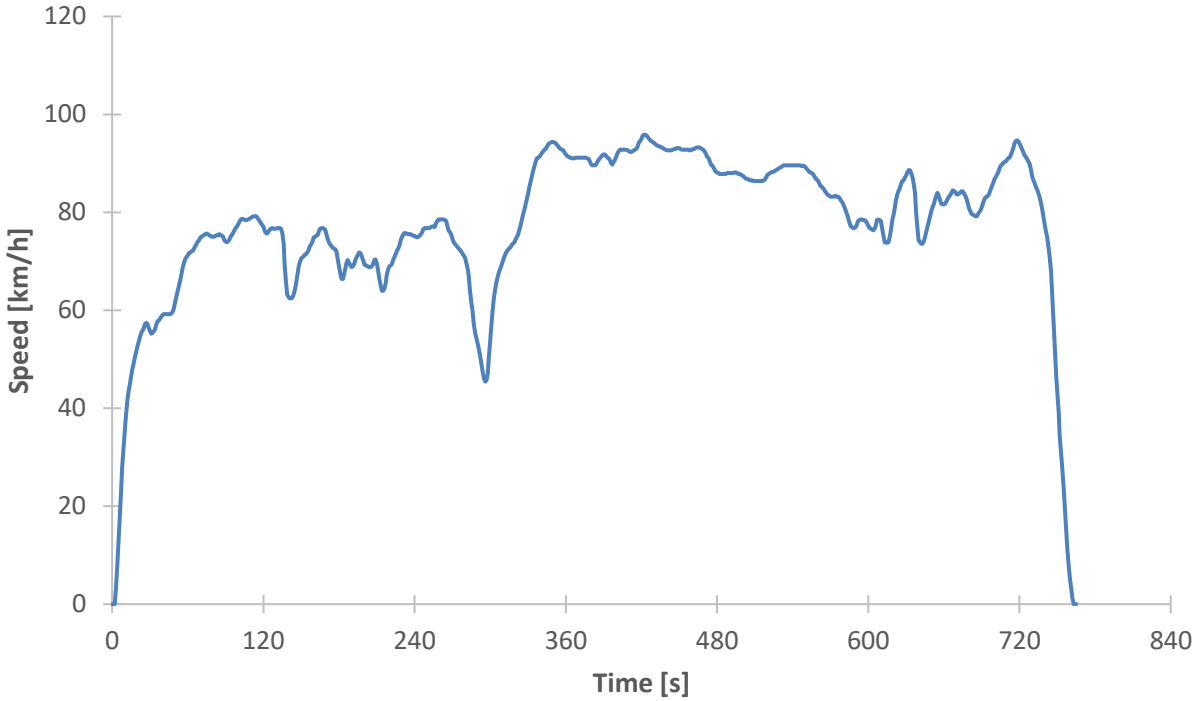

Figure 4: Speed profile of Highway drive cycle

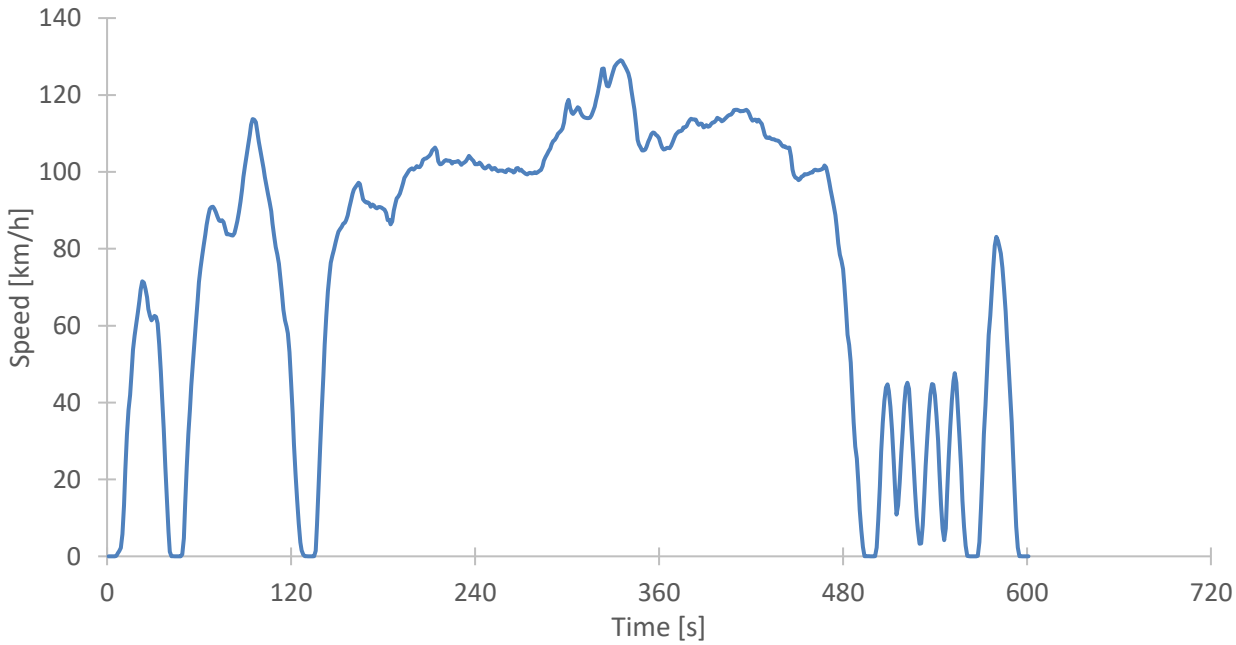

Figure 5: Speed profile of US06 drive cycle

A sensitivity analysis was conducted by varying the proportion of city and highway driving, as summarized in Table VI. This sensitivity analysis entailed weighing the city drive cycle by a factor, α and the highway drive cycle by a factor, $1 - \alpha$. The results demonstrate that when the proportion of city driving is 15% or higher, BEVs produce less non-exhaust $PM_{2.5}$ emissions

compared to ICEVs. This finding is attributed to the fact that while BEVs produce more tire related $PM_{2.5}$ emissions because of their extra weight, they also produce less brake $PM_{2.5}$ emissions when driving in a city environment where brakes are used more frequently. This conclusion also demonstrates the necessity of considering both brake and tire $PM_{2.5}$ emissions when comparing BEVs to ICEVs.

Table VI. Impact of proportion of city driving on non-exhaust PM2.5 emissions

City Cycle Weight	ICEV [mg]	BEV [mg]	Change [%]
0.00	12.63	15.77	25%
0.05	14.02	16.09	15%
0.10	15.41	16.42	7%
0.15	16.80	16.74	0%
0.20	18.19	17.07	-6%
0.25	19.58	17.39	-11%
0.30	20.97	17.72	-16%
0.40	23.75	18.37	-23%
0.50	26.53	19.02	-28%
0.60	29.31	19.67	-33%
0.70	32.09	20.32	-37%
0.80	34.87	20.97	-40%
0.90	37.65	21.62	-43%
1.00	40.43	22.27	-45%

4.2 Network Modeling Results

We tested the model on a 28-km section of the southbound direction of Interstate 81 (I-81) traveling from upstream of milepost 132 to downstream of milepost 118, as illustrated in Figure 6. The I-81 network that was modeled consists of 713 nodes, 496 links (roadway segments), and was assigned a demand of 5643 vehicles loaded over the duration of 1 hour at the 100% demand level. This demand was calibrated to observed conditions using count data that were conducted by the team. These count data were input to a synthetic origin-destination (OD) demand estimator, QUEENSOD to generate the most likely OD that matches the observed link flows as described in (Van Aerde, Rakha and Paramahamsan 2003). The simulation network construction involved building a network from an AutoCAD design (Rakha, et al. 2005). This design was used to configure the horizontal profile with a high degree of accuracy. The roadway grades for each link was generated by driving a Global Positioning System (GPS) equipped vehicle with a along the network. The section is mountainous and includes grades of up to 4% over a few kilometres, as illustrated in Figure 6. Given the significant grades, the high free-flow speed (112 km/h), and low demand level, this section of freeway is expected to favour ICEVs.

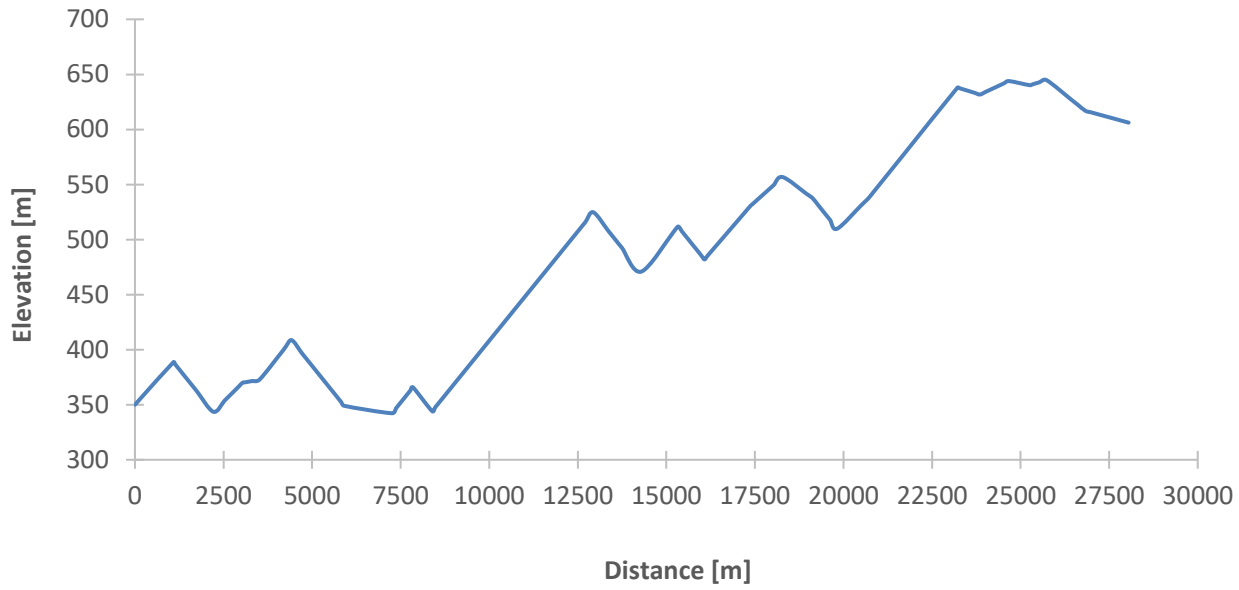

Figure 6. Vertical profile of simulated I-81 section (travel from left to right)

The fundamental diagram parameters: lane saturation flow rate, free-flow speed, speed-at-capacity, and jam density were derived based on the Highway Capacity Manual (HCM) for a typical freeway section (National Academies of Sciences 2022). While the counts included trucks, for simplicity we modelled all vehicles as light duty vehicles.

In this analysis, the volume-to-capacity ratio was varied by varying the demand level from 1% to 100% of the peak demand, and the non-exhaust $PM_{2.5}$ and exhaust CO_2 emissions were quantified. We ran two scenarios: the first with all the vehicles as ICEVs (2024 Toyota Camry) and the second with all vehicles as BEVs (2024 Tesla model S). The various vehicle parameters that were used are provided in Table VII.

Table VII. Vehicle parameters used in the simulation runs

Parameter	2024 Toyota Camry	2024 Tesla Model S
Vehicle weight (kg)	1501	2068
Vehicle length (meters)	4.88	5.02
Proportion of mass on tractive axle	0.6	0.6
Coefficient of friction	0.5	0.5
Vehicle gas/diesel engine power [KW]	151.4	0.00
Maximum battery energy for eclectic motor [KW]	0.00	499.60
Driveline efficiency	0.92	0.92
Drag coefficient	0.31	0.208
Frontal area [m^2]	2.126	2.27
Rolling coefficient	1.75	1.75
First rolling resistance constant	0.0328	0.0328
Second rolling resistance constant	4.575	4.575
Battery efficiency for electric vehicles	0.00	0.90
Minimum state of charge for electric vehicles	0.00	0.21
Maximum state of charge for electric vehicles	0.00	0.95
Initial state of charge	0.00	0.95
Electric motor efficiency for electric vehicles	0.00	0.91
Regenerative efficiency for electric vehicles	0.00	1.00
Battery capacity (kWh) for electric vehicles	0.00	99.30
Power consumed by auxiliaries (kW)	0.00	0.10
The VT-CPFM/VT-CPEM model parameter Alpha_0	3.908E-04	2.778E-05
The VT-CPFM/VT-CPEM model parameter Alpha_1	5.870E-05	1.840E-04
The VT-CPFM/VT-CPEM model parameter Alpha_2	1.000E-08	1.890E-06

The results, as illustrated in Figure 7, demonstrate that for this specific network, at a volume-to-capacity ratio of at least 25% (demand level of at least 32% of the peak demand), BEV $PM_{2.5}$ emissions fall below ICEV $PM_{2.5}$ emissions. In other words, when the freeway has minimal traffic demand, BEVs emit more $PM_{2.5}$ non-exhaust emissions, but as traffic increases, this trend reverses.

The key findings of these simulation runs can be summarized as follows: 1) At volume-to-capacity ratios below 25% (demand levels below 32% of the peak), BEVs emit more $PM_{2.5}$ non-exhaust emissions than ICEVs because of the increased tire wear caused by the heavier weight of BEVs. 2) As the volume-to-capacity ratio increases to at least 25%, BEV $PM_{2.5}$ emissions become lower than those of ICEVs because of the effective use of regenerative braking in BEVs, which reduces brake wear and thus brake PM emissions significantly. 3) The crossover point at around 25% indicates that BEVs become environmentally advantageous in terms of $PM_{2.5}$ emissions as traffic conditions intensify. 4) Throughout the range of volume-to-capacity ratios, BEVs consistently produce no CO_2 emissions compared to ICEVs, reinforcing the overall lower greenhouse gas emissions from BEVs. The average of ICEV CO_2 emissions in gm/vehicle was found to increase linearly as a function of the volume-to-capacity ratio ($v/c = [0,1]$), as shown

in Eqn. (31). This linear relationship is strongly supported by the data, with a high coefficient of determination ($R^2 = 0.996$). The equation demonstrates a linear increase in the ICEV average CO_2 emissions as the volume-to-capacity ratio increases. BEVs, on the other hand, emit no CO_2 emissions while driving.

$$CO_2 = 3553.2 + 607.56\frac{v}{c} \quad (31)$$

The analysis underscores the dynamic nature of non-exhaust PM emissions based on volume-to-capacity ratios. While BEVs may emit more $PM_{2.5}$ under very low traffic conditions due to higher tire wear, they emit less $PM_{2.5}$ as traffic increases, owing to the benefits of regenerative braking. Furthermore, the linear increase in ICEV CO_2 emissions with traffic demand underscores the efficiency advantage of BEVs in all conditions, but more in congested conditions (Figure 8). This finding is crucial for understanding the environmental impact of BEVs in different traffic scenarios and supports the argument for their efficiency in urban and high-traffic environments where their advantages are maximized.

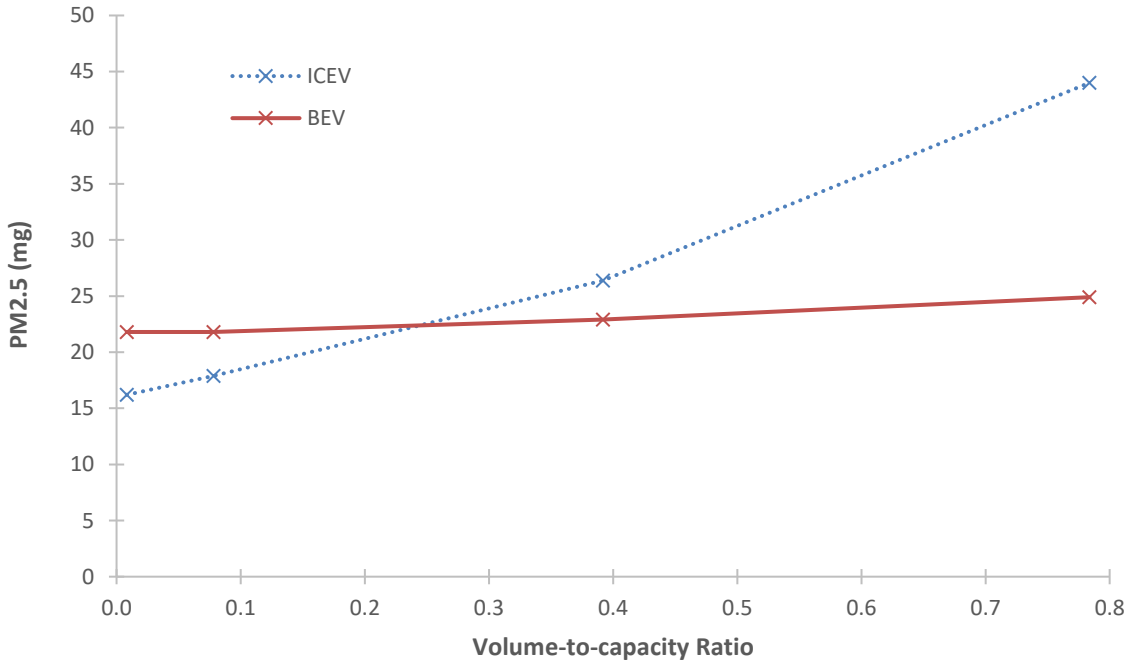

Figure 7. Non-exhaust PM2.5 emissions for I-81 road network simulations for ICEVs and BEVs.

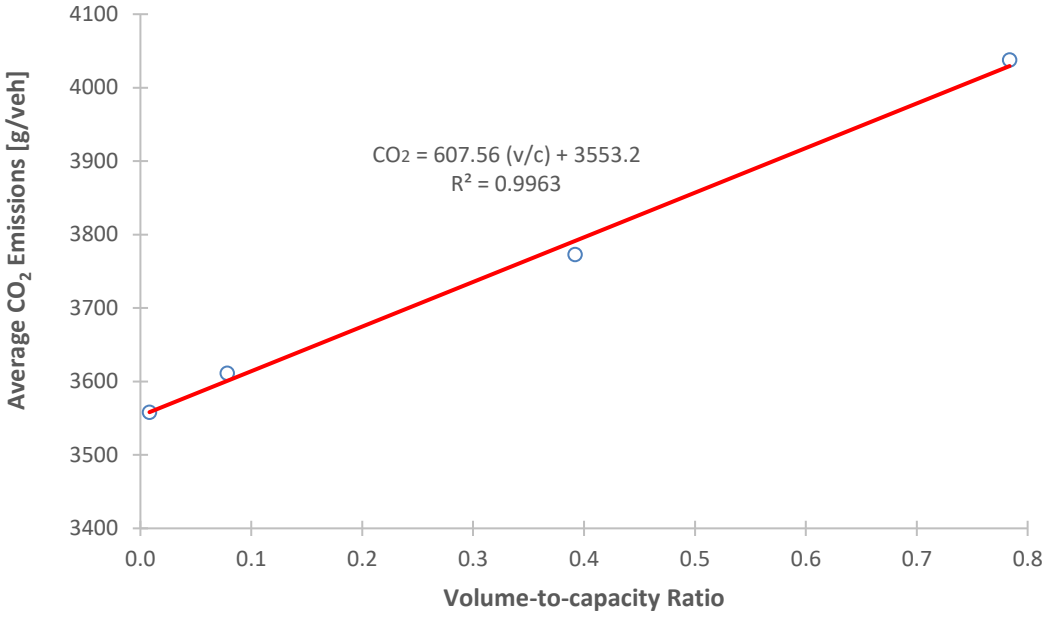

Figure 8. Variation in ICEV CO_2 emissions as a function of the volume-to-capacity ratio on the I-81 roadway section

5. CONCLUSIONS AND RECOMMENDATIONS FOR FUTURE WORK

The study demonstrates the necessity of considering both tire and brake PM emissions to accurately compare the environmental impact of BEVs and ICEVs. We found that BEVs tend to have lower non-exhaust PM emissions in mixed driving conditions (city and freeway) and always have lower exhaust greenhouse gas emissions. This comprehensive modeling approach helps clarify the debate and supports the argument for the environmental advantages of BEVs.

By incorporating these detailed models into traffic simulations, the study provides a tool that policymakers and transportation planners may use to better understand and manage vehicle emissions at a city level. This tool can inform strategies to reduce overall vehicular pollution and promote sustainable transportation solutions.

As is the case with any study, future work is needed to build on the findings and improve the robustness of the models. Proposed future work includes the following: 1) Gather real-world data to validate the current brake and tire emission models. 2) Potentially develop new models based on these empirical data to enhance accuracy and reliability. 3) Apply and test the models on various traffic networks and under different demand levels. 4) Include a wider range of vehicle types in the analysis, such as sport utility vehicles (SUVs), to assess the emissions for different categories of BEVs and ICEVs. These steps will help refine the models, ensure their applicability across different scenarios, and provide a more comprehensive understanding of vehicle emissions. This future work will support more informed decision-making for policymakers aiming to reduce vehicular emissions and promote sustainable transportation systems.

ACKNOWLEDGEMENTS

This study has been partially supported by the Center for Tire Research (CenTiRe), a National Science Foundation Industry/University Cooperative Research Center (I/UCRC) at Virginia Tech, and the Sustainable Mobility and Accessibility Regional Transportation Equity Research (SMARTER) Center.

REFERENCES

Alemayehu, Y.A., S.L. Asfaw, and T.A. Terfie. 2020. "Exposure to urban particulate matter and its association with human health risks." *nvironmental Science and Pollution Research* 27: 27491–27506. doi:10.1007/s11356-020-09132-1.

Alves, C. A., A. M. P. Vicente, A. I. Calvo, D. Baumgardner, F. Amato, X. Querol, C. Pio, and M. Gustafsson. 2020. "Physical and chemical properties of non-exhaust particles generated from wear between pavements and tyres." *Atmospheric Environment* 224: 117252.

Avgoustis, A., Hesham A Rakha, and M. Van Aerde. 2004. "Framework for Estimating Network-wide Safety Impacts of Intelligent Transportation Systems." *Intelligent Transportation Systems Safety and Security Conference.* Miami.

Beddows, D. C., and R. M Harrison. 2021. "PM10 and PM2. 5 emission factors for non-exhaust particles from road vehicles: Dependence upon vehicle mass and implications for battery electric vehicles." *Atmospheric Environment* 244.

Bondorf, L., L. Köhler, T. Grein, F. Epple, F. Philipps, M. Aigner, and T. Schripp. 2023. "Airborne brake wear emissions from a battery electric vehicle." *Atmosphere* 14 (3): 488.

Dion, Francois, Hesham A. Rakha, and Youn-Soo Kang. 2004. "Comparison of delay estimates at under-saturated and over-saturated pre-timed signalized intersections." *Transportation Research Part B-methodological* 38 (2): 99-122. Accessed 5 21, 2024. https://sciencedirect.com/science/article/pii/s0191261503000031.

Du, J., H.A. Rakha, A. Elbery, and M. Klenk. 2018. "Microscopic Simulation and Calibration of a Large-Scale Metropolitan Network: Issues and Proposed Solutions." *Transportation Research Board 97th Annual Meeting.* Washington DC.

Elbery, A., Y. Bichiou, H.A. Rakha, J. Du, F. Dvorak, and M. Klenk. 2018. "City-level Agent-based Multi-modal Modeling of Transportation Networks: Model Development and Preliminary Testing." In *Smart Cities, Green Technologies, and Intelligent Transport Systems*.

Emissions_Analytics. 2024. *Do No Harm.* Accessed 5 22, 2024. https://www.emissionsanalytics.com/news/do-no-harm.

EPA. 2014. *Overview of EPA's MOtor Vehicle Emission Simulator (MOVES3).* Washington DC: Assessment and Standards Division, Office of Transportation and Air Quality, U.S. Environmental Protection Agency.

Fadhloun, Karim, and Hesham A. Rakha. 2019. "A novel vehicle dynamics and human behavior car-following model: Model development and preliminary testing." *International journal of transportation science and technology.* Accessed 5 22, 2024. https://sciencedirect.com/science/article/pii/s2046043018301631.

Fadhloun, Karim, Hesham A. Rakha, Abdessattar Abdelkefi, and Amara Loulizi. 2017. *An Enhanced Rakha-Pasumarthy-Adjerid Car-Following Model Accounting for Driver Behavior.* Accessed 5 22, 2024. https://trid.trb.org/view/1437242.

Farag, M.M.G., H.A. Rakha, E.A. Mazied, and J. Rao. 2021. "INTEGRATION Large-Scale Modeling Framework of Direct Cellular Vehicle-to-All (C-V2X) Applications." *Sensors* 21. doi:10.3390/s21062127.

Fiori, Chiara, Kyoungho Ahn, and Hesham A Rakha. 2016. "Power-based Electric Vehicle Energy Consumption Model: Model Development and Validation." *Journal of Applied Energy* 168: 257-268.

Harrison, R. M., J. Allan, D. Carruthers, M. R. Heal, A. C. Lewis, B. Marner, T. Murrells, and A. Williams. 2021. "Non-exhaust vehicle emissions of particulate matter and VOC from road traffic: A review." *Atmospheric Environment* 262: 118592.

Kim, K.H., E. Kabir, and S. Kabir. 2015. "A review on the human health impact of airborne particulate matter." *Environment International* 74: 136-143.

National Academies of Sciences, Engineering, and Medicine. 2022. *Highway Capacity Manual 7th Edition: A Guide for Multimodal Mobility Analysis.* Washington, DC, DC: The National Academies Press. doi:10.17226/26432.

Oroumiyeh, F., and Y. Zhu. 2021. "Brake and tire particles measured from on-road vehicles: Effects of vehicle mass and braking intensity." *Atmospheric Environment: X* 12: 100121.

Piscitello, A., C. Bianco, A. Casasso, and R. Sethi. 2021. "Non-exhaust traffic emissions: Sources, characterization, and mitigation measures." *Science of the Total Environment* 766: 144440.

Rakha, H., A. Medina, K. Ahn, I. El-Shawarby, and M. Arafeh. 2005. "Evaluating Alternative Lane Management Strategies along I-81." *Transportation Research Record* 1925: 76-86. doi:10.1177/0361198105192500109.

Rakha, Hesham A. 2024. *INTEGRATION © Release 2.40 for Windows: User's Guide – Volume I: Fundamental Model Features.* Blacksburg: Virginia Tech.

—. 2024. *INTEGRATION © Release 2.40 for Windows: User's Guide – Volume II: Advanced Model Features.* Blacksburg: Virginia Tech.

Rakha, Hesham A. 2009. "Validation of Van Aerde's Simplified Steady-state Car-following and Traffic Stream Model." *Transportation Letters: The International Journal of Transportation Research* 1 (3): 227-244. doi:10.3328/TL.2009.01.03.227-244.

Rakha, Hesham A, and Mazen Arafeh. 2009. "Calibrating Steady-State Traffic Stream and Car-following Models using Loop Detector Data." *Transportation Science* 44 (2). doi:10.1287/trsc.1090.0297.

Rakha, Hesham A, Kyoungho Ahn, Kevin Moran, Bart Saerens, and Erik Van den Bulck. 2011. "Virginia Tech Comprehensive Power-based Fuel Consumption Model: Model Development and Testing." *Transportation Research Part D: Transport and Environment* 16 (7): 492-503. doi:10.1016/j.trd.2011.05.008.

Rakha, Hesham A., and Kyoungho Ahn. 2004. "Integration modeling framework for estimating mobile source emissions." *Journal of Transportation Engineering-asce* 130 (2): 183-193. Accessed 5 21, 2024. https://trid.trb.org/view/699423.

Rakha, Hesham A., and Yihua Zhang. 2004. "INTEGRATION 2.30 Framework for Modeling Lane-Changing Behavior in Weaving Sections." *Transportation Research Record* 1883 (1883): 140-149. Accessed 5 21, 2024. https://trrjournalonline.trb.org/doi/abs/10.3141/1883-16.

Rakha, Hesham A., Kyoungho Ahn, and Kevin Moran. 2012. "INTEGRATION Framework for Modeling Eco-routing Strategies: Logic and Preliminary Results." *International journal*

of transportation science and technology 1 (3): 259-274. Accessed 5 21, 2024. https://sciencedirect.com/science/article/pii/s2046043016301629.

Rakha, Hesham A., Youn-Soo Kang, and Francois Dion. 2001. "Estimating vehicle stops at undersaturated and over saturated fixed-time signalized intersections." *Transportation Research Record* (1776): 128-137. Accessed 5 21, 2024. http://researchgate.net/profile/hesham_rakha/publication/254391725_estimating_vehicle_stops_at_undersaturated_and_oversaturated_fixed-time_signalized_intersections/links/0c960534f272c2a31d000000.pdf.

Rødland, E. S., M. Gustafsson, D. Jaramillo-Vogel, I. Järlskog, K. Müller, C. Rauert, J. Rausch, and S. Wagner. 2023. "Analytical challenges and possibilities for the quantification of tire-road wear particles." *TrAC Trends in Analytical Chemistry* 11721.

Sisani, Federico, Francesco Di Maria, and Daniela Cesari. 2022. "Environmental and human health impact of different powertrain passenger cars in a life cycle perspective. A focus on health risk and oxidative potential of particulate matter components." *Science of The Total Environment* 805. doi:10.1016/j.scitotenv.2021.150171.

Timmers, V.R., and P.A. Achten. 2016. "Non-exhaust PM emissions from electric vehicles." *Atmospheric Environment* 134: 10-17.

Van Aerde, M., H. Rakha, and H. Paramahamsan. 2003. "Estimation of O-D Matrices: The Relationship between Practical and Theoretical Considerations ." *Transportation Research Record* 1831: 122-130. doi:10.3141/1831-14.

Wang, Jinghui, Hesham A Rakha, and Karim Fadhloun. 2017. *Comparison of Car-Following Models: A Vehicle Fuel Consumption and Emissions Estimation Perspective.* Accessed 5 22, 2024. https://trid.trb.org/view/1437499.

Wang, Jinghui, Hesham A Rakha, and Karim Fadhloun. 2017. "Validation of the Rakha-Pasumarthy-Adjerid car-following model for vehicle fuel consumption and emission estimation applications." *Transportation Research Part D-transport and Environment* 55: 246-261. Accessed 5 22, 2024. https://sciencedirect.com/science/article/pii/s1361920916306654.

Zhang, Q., J. Yin, T. Fang, Q. Guo, J. Sun, J. Peng, and H. Mao. 2024. "Regenerative braking system effectively reduces the formation of brake wear particles." *Journal of Hazardous Materials* 465.

Zhang, Qijun, Tiange Fang, Zhengyu Men, Ning Wei, Jianfei Peng, Tianqiang Du, Xinfeng Zhang, Yao Ma, Lin Wu, and Hongjun Mao. 2024. "Direct measurement of brake and tire wear particles based on real-world driving conditions." *Science of the Total Environment* 906. doi:10.1016/j.scitotenv.2023.167764.

APPENDIX

Regression Statistics	
Multiple R	0.9686
R Square	0.9382
Adjusted R Square	0.9074
Standard Error	0.4074
Observations	4

ANOVA

	df	*SS*	*MS*	*F*	*Significance F*
Regression	1	5.043	5.043	30.388	0.031
Residual	2	0.332	0.166		
Total	3	5.375			

	Coefficients	*Standard Error*	*t Stat*	*P-value*	*Lower 95%*	*Upper 95%*
Intercept	-2.730700	1.5069	-1.8121	0.2117	-9.2144	3.7530
X Variable 1	0.002974	0.0005	5.5125	0.0314	0.0007	0.0053

Figure 9. Regression results considering an intercept

Regression Statistics	
Multiple R	0.9965
R Square	0.9931
Adjusted R Square	0.6597
Standard Error	0.5406
Observations	4

ANOVA

	df	*SS*	*MS*	*F*	*Significance F*
Regression	1	125.498	125.498	429.362	0.002
Residual	3	0.877	0.292		
Total	4	126.375			

	Coefficients	*Standard Error*	*t Stat*	*P-value*	*Lower 95%*	*Upper 95%*
Intercept	0	#N/A	#N/A	#N/A	#N/A	#N/A
X Variable 1	0.002005019	9.676E-05	2.072E+01	2.458E-04	1.697E-03	2.313E-03

Figure 10. Regression results considering an intercept of zero